Transit f(Q, T) Gravity Model with Specific Hubble's Parameter: An Observational Constraints

A. P. Kale , Y. S. Solanke , S. H. Shekh , Anirudh Pradhan *

Posted Date: 8 August 2023

doi: 10.20944/preprints202308.0625.v1

Keywords: Cosmological models; f(Q, T) gravity; Observational Constraints; FLRW space-time; Deceleration parameter q; Root Mean Square Error (RMSE)

Article

Transit $f(Q,T)$ Gravity Model with Specific Hubble's Parameter: An Observational Constraints

A. P. Kale [1], Y. S. Solanke [2], S. H. Shekh [3] and Anirudh Pradhan [4,*]

1 Department of Mathematics, M. M. Mahavidyalaya, Darwha, Yavatmal 445202, India; akshaykale1000@gmail.com
2 Department of Mathematics, Mungasaji Maharaj Mahavidyalaya, Darwha, Yavatmal 445202, India; yadaosolanke@gmail.com
3 Department of Mathematics, S.P.M. Science and Gilani Arts, Commerce College, Ghatanji, Dist. Yavatmal, Maharashtra 445301, India; da_salim@rediff.com
4 Centre for Cosmology, Astrophysics and Space Science, GLA University, Mathura-281406,U.P., India
* Correspondence: pradhan.anirudh@gmail.com

Abstract: The present analysis deals with the study of the $f(Q,T)$ theory of gravity which was recently considered by many cosmologists. In this theory of gravity, the action is taken as an arbitrary function $f(Q,T)$ where Q is non-metricity and T is the trace of energy-momentum tensor for matter fluid. In this study, we have taken three different forms of the function $f(Q,T)$ as $f(Q,T) = a_1Q + a_2T$ and $f(Q,T) = a_3Q^2 + a_4T$ and discussed some physical properties of the same. Also, we have obtained the various cosmological parameters towards Friedmann-Lemaitre-Robertson-walker (FLRW) Universe by defining the transit form of scale factor which yields the Hubble parameter in redshift form as $H(z) = \frac{H_0}{(\lambda+1)}\left(\lambda + (1+z)^{\delta}\right)$. By applying the Root Mean Squared Error formula (RMSE), we were able to determine the approximate best-fit values of model parameters using the least square approach for observational constraints on the datasets Hubble dataset $H(z)$, Supernova dataset SNe-Ia, etc. We have observed that the deceleration parameter $q(z)$ exhibits a signature-flipping (transition) point within the range $0.623 \leq z_0 \leq 1.668$ through which it changes its phase from the decelerated to the accelerated expanding universe with $\omega = -1$ at $z = -1$ for the approximate best-fit values of the model parameters.

Keywords: cosmological models; $f(Q,T)$ gravity; observational constraints; FLRW space-time; deceleration parameter q; Root Mean Square Error (RMSE)

PACS: 98.80-k; 98.80.JK; 04.50.Kd

I. Introduction

The most successful theory, according to the new observation, is Einstein's theory of general relativity but it has some limitations to explain the phenomenon like the Big Bang singularity, general relativity not respecting local black holes, a consistent quantum gauge field theory of gravity, etc. The data provide compelling evidence that our universe is going through an expansion phase as well as an acceleration phase, according to [1–3]. For an understanding of the universe is accelerating in an organized way, from time to time various cosmologists have proposed some well-known modified theories of gravity like $f(G)$ gravity [4], $f(R)$ gravity [5–7], $f(R,T)$ [8–14], $f(\tau)$ gravity [15], $f(G,T)$ gravity [16], $f(R,T,R_{\mu\upsilon}T^{\mu\upsilon})$ gravity [17], $f(Q)$ gravity [18–25] and recently proposed $f(Q,T)$ [26–30] gravity. Dark energy and Dark matter refer back to the unseen additives of the Universe. Dark matter is an invisible, non-baryonic matter believed to give an explanation of phenomena including gravitational lensing and galactic rotation curves. Dark energy is responsible for the accelerating expansion of the Universe [31,32].

Geometric variables in symmetric teleparallel gravity reflected the gravitational interaction's physical characteristics, which are symbolised by the metric's non-metricity Q. The non-metricity tensor is the covariant derivative of the metric tensor. This strategy was first presented by Nester

Preprints (www.preprints.org) | NOT PEER-REVIEWED | Posted: 8 August 2023 doi:10.20944/preprints202308.0625.v1

and Yo [18]. The Lagrangian is viewed as an arbitrary function of the non-metricity in an extension of symmetric teleparallel gravity. According to Xu's gravity theory [26], Q and the trace of the matter-energy momentum tensor T are $f(Q,T)$. As in $f(R,T)$, they cause the cosmos to undergo some large thermodynamic changes [8].

We are studying various energy conditions in the recently proposed $f(Q,T)$ gravity theory in the present work. Energy conditions play a vital role in defining cosmological evolution, the emergence of Big-Rip Singularities, and Black hole dynamics [33].It explains how geodesics behave in ways that are similar to space, time, or light. It allows us some latitude in our analysis of particular notions about the nature of cosmic geometries and particular relationships that energy momentum must satisfy under stress in order for energy density to be positive. It is typically used in general relativity to illustrate and investigate space-time singularities [34]. Using power law in $f(R)$ gravity Capozziello studied the energy condition [35]. The Null Energy Condition requires for Black hole thermodynamics [33], whereas the Hawking-Penrose singularity theorem invokes Weak Energy Condition and Strong Energy Condition [36]. M. Sharif [37] introduced energy conditions using FLRW universe for two models. The viability of the bounds in $f(R,\Box R,T)$ is investigated through energy conditions in [38]. In different modified theories of gravity like $f(R)$ and generalized teleparallel theory, energy conditions have been investigated [39–42].

Motivated from the above analysis and discussion in the present investigation we investigate the two different $f(Q,T)$ models in a flat FLRW space-time with proposed equation of state (EoS) $p=\omega\rho$, deceleration parameter (q) where p, ρ and ω represent cosmological pressure, energy density and EoS parameter along with the validation of energy conditions.

The organisation of the analysis is as follows: The fundamental formalism of the $f(Q,T)$ theory of gravity by changing action is presented in Section II. The gravitational field equations and the emergent scale factor are shown in Section III.While the empirical constraints that explain model-free parameters are offered in Section IV. In Section V cosmological parameters are covered. In Section VI, a few models of "f(Q,T)" gravity are discussed. We have taken a function $f(Q,T)$ both linear and quadratic as $f(Q,T)=a_1Q+a_2T$ and $f(Q,T)=a_3Q^2+a_4T$ where a_1, a_2, a_3 and a_4 are model parameters. A summary of concluding remarks is provided in the last Section VII.

II. Basic formalism in $f(Q,T)$ gravity

The modified Einstein-Hilbert action principle for the $f(Q,T)$ extended symmetric teleparallel gravity is given by [26]

$$S=\int\left[\frac{1}{16\pi}f(Q,T)+L_m\right]\sqrt{-g}d^4x, \tag{1}$$

where $f(Q,T)$ being the general functional form of the non-metricity scalar Q and the trace of the energy-momentum tensor T. g is the determinant of the metric tensor $g_{\mu\nu}$ i.e. $g=\det\left(g_{\mu\nu}\right)$, and L_m is Lagrangian matter. The non-metricity scalar Q is defined as

$$Q\equiv-g^{\mu\nu}\left(L^{\delta}{}_{\alpha\mu}L^{\alpha}{}_{\nu\delta}-L^{\delta}{}_{\alpha\delta}L^{\alpha}{}_{\mu\nu}\right), \tag{2}$$

where the deformation tensor $L^{\delta}{}_{\alpha\gamma}$ is given by

$$L^{\delta}{}_{\alpha\gamma}=-\frac{1}{2}g^{\delta\eta}\left(\nabla_\gamma g_{\alpha\eta}+\nabla_\alpha g_{\eta\gamma}-\nabla_\eta g_{\alpha\gamma}\right). \tag{3}$$

The non-metricity tensor has the following definition:

$$Q_{\gamma\mu\nu}=\nabla_\gamma g_{\mu\nu}, \tag{4}$$

Preprints (www.preprints.org) | NOT PEER-REVIEWED | Posted: 8 August 2023 doi:10.20944/preprints202308.0625.v1

and the non-metricity tensor's trace is derived as

$$Q_\delta = g^{\mu\nu} Q_{\delta\mu\nu}, \quad \widetilde{Q}_\delta = g^{\mu\nu} Q_{\mu\delta\nu}. \tag{5}$$

Further, define the super potential tensor as follows

$$P^\delta_{\mu\nu} = -\frac{1}{2} Q^\delta_{\mu\nu} + \frac{1}{4}\left(Q^\delta - \widetilde{Q}^\delta\right) g_{\mu\nu} - \frac{1}{4}\delta^\delta_{(\mu} Q_{\nu)}, \tag{6}$$

using this the non-metricity scalar is

$$Q = -Q_{\delta\mu\nu} P^{\delta\mu\nu}. \tag{7}$$

The variation of the energy-momentum tensor with respect to the metric tensor $g_{\mu\nu}$ read as

$$\frac{\delta(g^{\mu\nu} T_{\mu\nu})}{\delta g^{\alpha\beta}} = T_{\alpha\beta} + \theta_{\alpha\beta}. \tag{8}$$

where the energy-momentum tensor is

$$T_{\mu\nu} = \frac{-2}{\sqrt{-g}} \frac{\delta\left(\sqrt{-g} L_m\right)}{\delta g^{\mu\nu}}, \tag{9}$$

and

$$\theta_{\mu\nu} = g^{\alpha\beta} \frac{\delta T_{\alpha\beta}}{\delta g^{\mu\nu}}. \tag{10}$$

Also, the field equations of $f(Q,T)$ gravity are given by varying the action, Equation (1), with respect to the metric tensor $g_{\mu\nu}$,

$$-\frac{2}{\sqrt{-g}} \nabla_\delta \left(f_Q \sqrt{-g} P^\delta{}_{\mu\nu}\right) - \frac{1}{2} f g_{\mu\nu} + f_T \left(T_{\mu\nu} + \theta_{\mu\nu}\right) - f_Q \left(P_{\mu\delta\alpha} Q_\nu{}^{\delta\alpha} - 2 Q^{\delta\alpha}{}_\mu P_{\delta\alpha\nu}\right) = 8\pi T_{\mu\nu}, \tag{11}$$

where $f_Q = \frac{df(Q,T)}{dQ}$, $f_T = \frac{df(Q,T)}{dT}$, and ∇_δ denotes the covariant derivative. From Equation (11) it emerge that the field equations of $f(Q,T)$ depend on the tensor $\theta_{\mu\nu}$. Various cosmological models of $f(Q,T)$ gravity, depending on the nature of the source of matter are possible. Very recently Koussour et al. [43] have investigated the quintessence form of extended symmetric teleparallel gravity with cosmic acceleration by assuming the cosmic time-redshift relation as $t(z) = \frac{nt_0}{m} g(z)$ which gives the Hubble parameter and verify the sustainability of the results through the energy conditions along with jerk parameter. Also, in [44] the authors investigated energy conditions in $f(Q,T)$ gravity for two different forms of models.

III. Flat FLRW Universe in $f(Q,T)$ cosmology

In order to find a solution for the field equations in $f(Q,T)$ extended symmetric teleparallel gravity, some straightforward assumptions, such as the selection of a metric, are frequently required. Consequently, we consider the form's flat FLRW metric,

$$ds^2 = -dt^2 + a^2(t)\left(dx^2 + dy^2 + dz^2\right), \tag{12}$$

where $a(t)$ is the scale factor of the metric and its depends on cosmic time (where unit of the cosmic time is Gyr). Energy-momentum tensor for the Universe, imagine to be behaves like a perfect fluid is given by

$$T^\mu_\nu = diag\left(-\rho, p, p, p\right), \tag{13}$$

Preprints (www.preprints.org) | NOT PEER-REVIEWED | Posted: 8 August 2023 doi:10.20944/preprints202308.0625.v1

Here, p denotes pressure and ρ denotes energy density of the Universe. Thus, for tensor θ_{ν}^{μ}, the expression is obtained as $\theta_{\nu}^{\mu} = diag\,(2\rho + p, -p, -p, -p)$. The Einstein field equations using the metric (12) are given as,

$$\kappa^2\rho = \frac{f}{2} - 6FH^2 - \frac{2\widetilde{G}}{1+\widetilde{G}}\left(\dot{F}H + F\dot{H}\right), \tag{14}$$

$$\kappa^2 p = -\frac{f}{2} + 6FH^2 + 2\left(\dot{F}H + F\dot{H}\right). \tag{15}$$

Hence overhead $(\cdot)$ represents a derivative with respect to cosmic time (t). In this case, $F \equiv f_Q$ and $\kappa^2\widetilde{G} \equiv f_T$ represent differentiation of function $f(Q,T)$ with respect to Q and T respectively and $Q = 6H^2$. With the help of Equations (14) and (15), the EoS parameter is expressed as

$$\omega = -1 + \left(\frac{1}{\kappa^2\rho}\right)\left(\frac{2\kappa^2 + f_T}{\kappa^2 + f_T}\right)\left(\dot{F}H + F\dot{H}\right). \tag{16}$$

A. Specific Hubble's parameters and analysis

Now we provide a glimpse on the main features of the scale factor (transit scale factor) and derive a few physical quantities from them to discuss the observed scenario. Hence for the transit scale factor, Hubble's parameter is observed as

$$H(z) = \epsilon\left(a^{-\delta} + \lambda\right). \tag{17}$$

where ϵ, λ and δ are the model parameters. Keep in mind the relation of a and z as $a = \frac{1}{1+z}$, Equation (17) becomes

$$H(z) = \frac{H_0}{(\lambda+1)}\left(\lambda + (1+z)^{\delta}\right). \tag{18}$$

here H_0 represents the present Hubble constant which explains the present expansion rate of the Universe. Freedman et al. [45] and Suyu et al. [46] evaluated a value of the present Hubble constant $H_0 = 72 \pm 8km/s/Mpc$ and $69.7^{+4.9}_{-5}km/s/Mpc$ where as recently Plank gives $H_0 = 67.3 \pm 1.20km/s/Mpc$ [47].

Using the time-redshift differential relation $\frac{d}{dt} = -(1+z)H\frac{d}{dz}$, the first and second derivative of H is obtained as

$$\begin{aligned} \dot{H}(z) &= -\frac{\delta H_0^2(z+1)^{\delta}\left(\lambda + (z+1)^{\delta}\right)}{(\lambda+1)^2} \quad \text{and} \\ \ddot{H}(z) &= \frac{\delta^2 H_0^3(z+1)^{\delta}\left(\lambda + (z+1)^{\delta}\right)\left(\lambda + 2(z+1)^{\delta}\right)}{(\lambda+1)^3} \end{aligned} \tag{19}$$

It is interesting to observe and compare our investigated model with the recent observations by finding the best-fit values and the best-fit curve of the Hubble function towards the model parameters H_0, ϵ, λ, and δ with the recent observational datasets. Hence, here we used the most favorable Hubble and Supernovae SNe-Ia to constrain the said model parameter in the following section.

IV. Observational constraints

The accelerated expansion can be explained by a cosmological constant; alternative explanations, such as dynamical dark energy or modified gravity, can be investigated by looking at how they affect the history of the universe's late-time expansion or the development of its structures. In order to identify constant parameters, we used the Hubble and Supernova Ia Datasets in this research.

Preprints (www.preprints.org) | NOT PEER-REVIEWED | Posted: 8 August 2023 doi:10.20944/preprints202308.0625.v1

A. Hubble Datasets

We notice the observational constraints on the parameters $H_0 = \epsilon(\lambda + 1)$, δ and λ using the latest 54 data points of $H(z)$ in the red-shift range $0.07 \leq z \leq 2.4$ in which 28 points obtained using DA method, whereas 26 points using BAO. The values are presented in Table 2.

We have found best-fit curve of $H(z)$ with 54 data observed values shown in Table 2, using $R^2 - test$:

$$R^2 = 1 - \frac{\sum_1^{54}[(H_i)_{obs} - (H_i)_{th}]^2}{\sum_1^{54}[(H_i)_{obs} - (H_i)_{mean}]^2} \tag{20}$$

If $R^2 = 1$ shows an exact fit the values of model parameters H_0,$\delta$and λ with observational datasets. From Equation (17) we required $-1 < z$ and $\epsilon \neq 0$. To find the best-fit values of H_0 ,δ and λ we have restricted the parametric space $-1 < z$ and $\epsilon \neq 0$. We used error bars to represent the mean point and its deviation from the mean for 54 points of Hubble data-set and compared our model with the well-accepted Λ CDM model for $H_0 = 67.8 km/s/Mpc$, $\Omega_{\Lambda_0} = 0.7$ and $\Omega_{m_0} = 0.3$. We have obtained the best-fit plot for approx values $H_0 = 64.49^{+0.33}_{-0.32}$,$\delta = 1.54^{+0.02}_{-0.02}$ and $\lambda = 1.14^{0.068}_{-0.077}$ having maximum $R^2 = 0.9321$ with RMSE is 11.071 as shows in Figure 1. Therefore $H_0 = 64.4772^{+0.33}_{-0.32} km/s/Mpc$ with 6.79% away from exact fit. The Figure 3 show the $1-\sigma$ (dark blue shaded), $2-\sigma$ (Sky blue shaded) maximum likelihood contours in the H_0-δ, H_0-λ and λ-δ planes for Hubble Datasets.

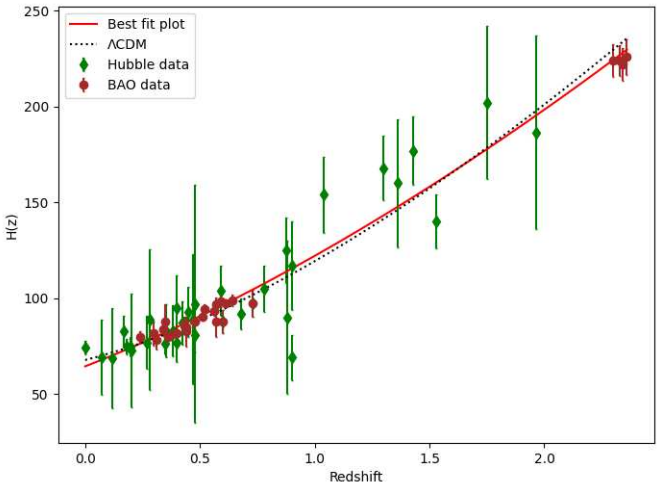

Figure 1. The best-fit plot for H(z) versus Redshift produced from the combined $H(z)$ + BAO Datasets is displayed in the figure.

B. Supernovae SNe-Ia

Distance modulus $\mu(z)$=$m - M$ given by

$$\mu(z) = 5\log_{10} d_L - 5\log_{10}(\frac{H_0}{Mpc}) + 25 \tag{21}$$

where M is constant for all SNe Ia. To obtain the best-fit curve we have to consider data frame having 580 entries observed of apparent magnitude from union 2.1 compilation [48] where $d_L(z) = (1+z)\int_0^z \frac{H_0}{H(z^*)} dz^*$. From the [48] statistically significant value of M is -19.30.

$$R^2 = 1 - \frac{\sum_1^{580}[(\mu_i)_{obs} - (\mu_i)_{th}]^2}{\sum_1^{580}[(\mu_i)_{obs} - (\mu_i)_{mean}]^2} \tag{22}$$

If $R^2 = 1$ shows exact fit the values of model parameters H_0 ,δ and λ with observational datasets. We used error bars to represent the mean point and its deviation from the mean for 580 points of SNe-Ia

Preprints (www.preprints.org) | NOT PEER-REVIEWED | Posted: 8 August 2023 doi:10.20944/preprints202308.0625.v1

Dataset and compared our model with the well-accepted Λ CDM model for $H_0 = 67.8km/s/Mpc$, $\Omega_{\Lambda_0} = 0.7$ and $\Omega_{m_0} = 0.3$. We have obtained the best-fit plot for approx values $H_0 = 68.665^{+2.2}_{-2.1}$,$\delta = 1.53^{+0.28}_{-0.29}$ and $\lambda = 1.86^{+0.37}_{-0.34}$ having maximum $R^2 = 0.9930$ with RMSE is 0.2662 as shows in Figure 2.

Therefore $H_0 = 68.665^{+2.2}_{-2.1} km/s/mpc$ with 0.7% away from exact fit. The Figure 3 show the $1-\sigma$ (dark green shaded), $2-\sigma$ (Light green shaded) maximum likelihood contours in the H_0-δ, H_0-λ and λ-δ planes for SNe-Ia Datasets.

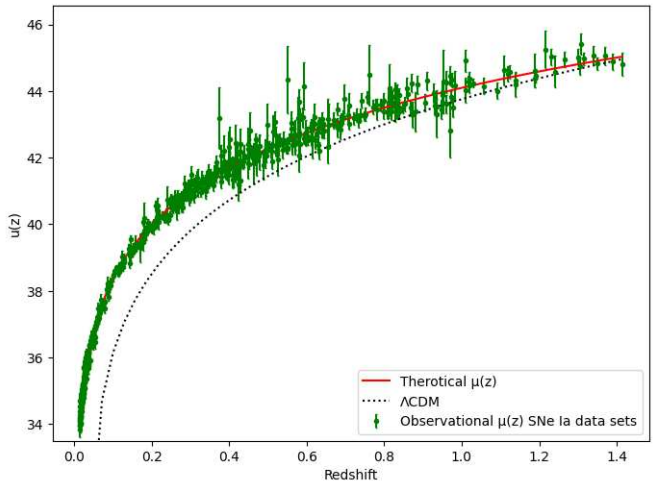

Figure 2. From the SNe-Ia Datasets, the graphic displays a best-fit plot of $\mu(z)$ vs Redshift.

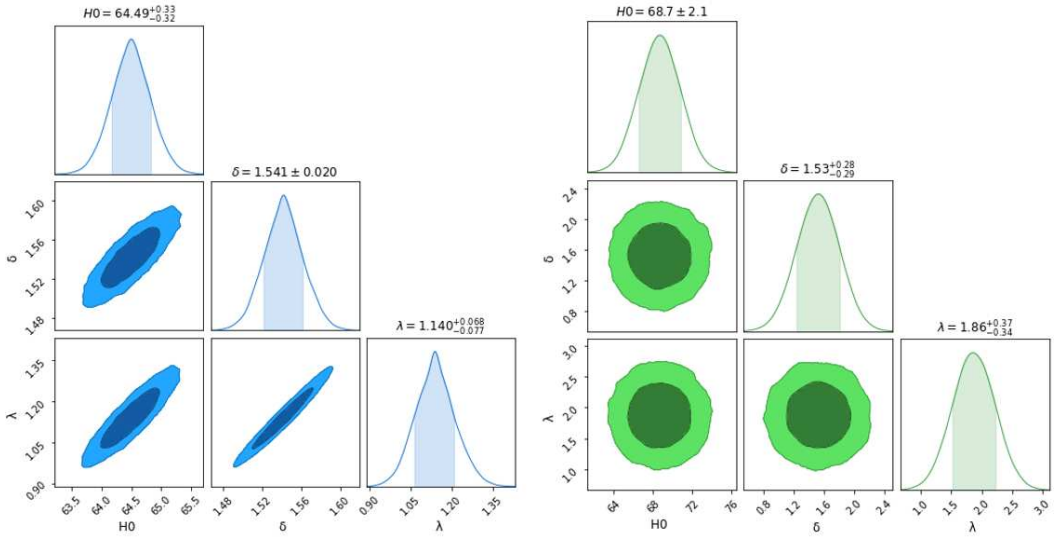

Figure 3. The $1-\sigma$ and $2-\sigma$ Maximum likelihood contours plots for the parameters using Observatory Hubble and SNe-Ia datasets.

V. Some cosmic parameters and energy conditions

Immediately, we accepted a set of solutions for the planned plan. In order to talk about how Universe is evolved in various phases, we need discuss the behavior of some cosmological parameters like the deceleration parameter, statefinder parameter etc., and these are defined as:

The deceleration parameter (q) is

$$q = -1 + \frac{d}{dt}\left(\frac{1}{H}\right) \tag{23}$$

Preprints (www.preprints.org) | NOT PEER-REVIEWED | Posted: 8 August 2023 doi:10.20944/preprints202308.0625.v1

Here the decelerating phase refers to $q > 0$ while $q < 0$ corresponds to the accelerating phase of the universe. for $q = 0$ is the transition point for the Universe from the deceleration to the acceleration phase.

The statefinder parameters are

$$r(z) = 1 + 3\frac{\dot{H}}{H^2} + \frac{\ddot{H}}{H^3} \quad \text{and} \quad s(z) = q + 2q^2 - \frac{\dot{q}}{H}. \tag{24}$$

The flat ΛCDM model is shown at the point where the statefinder parameters $\{r, s\} = \{1, 0\}$ have the corresponding values. Additionally, keep in mind that in the $\{r, s\}$ plane, a positive parameter s (i.e., $s > 0$) denotes a quintessence-like model of dark energy, whereas a negative parameter s (i.e., $s < 0$) denotes a phantom-like model of dark energy. Furthermore, by traversing the point $\{r, s\} = \{1, 0\}$, one can evolve from a phantom to the quintessence.

Energy conditions

One can derive highly potent and broad theorems regarding the behavior of massive gravitational fields and cosmic geometries using the energy conditions (ECs) of general relativity (GR). Generally speaking, ECs can be divided into

- Strong Energy Condition (SEC): Gravity should always be attractive and it formulated as $\rho + 3p \geq 0$.
- Dominant Energy Condition (DEC): When observer measures a matter energy density then will be positive and propagate in a causal way, which leads to $\rho \geq |p|$.
- Weak Energy Condition (WEC): The matter energy density measured by any observer should be positive, $\rho \geq 0, \rho + p \geq 0$.
- Null Energy Condition (NEC): It's the minimum requirement that is implied by SEC and WEC, is $\rho + p \geq 0$.

The violation of the NEC in the energy conditions implies that none of the energy criteria given are valid. The current fast expansion of the universe has raised questions about the SEC. In cosmological situations during the inflationary expansion and at the present, SEC must be broken.
Making use of Equations (18) and (19), the deceleration parameter and statefinder parameters are obtained as

$$q = -1 + \frac{\delta(z+1)^{\delta}}{\lambda + (z+1)^{\delta}}. \tag{25}$$

$$r(z) = \frac{\lambda^2 + (\delta - 2)(\delta - 1)\lambda(z+1)^{\delta} + (\delta - 1)(2\delta - 1)(z+1)^{2\delta}}{\left(\lambda + (z+1)^{\delta}\right)^2} \tag{26}$$

$$s(z) = 1 + \frac{\delta(z+1)^{\delta-1}\left((z+1)\epsilon\left((2\delta - 3)(z+1)^{\delta} - 3\lambda\right)\left(\lambda + (z+1)^{\delta}\right) - \delta\lambda\right)}{\epsilon\left(\lambda + (z+1)^{\delta}\right)^3}. \tag{27}$$

After analysing the SNe-Ia data by many researchers it was observed that datasets favour current acceleration for $(z < 0.5)$ and past deceleration for $(z > 0.5)$. A little while back, according to the high-z supernova search (HZSNS) team $z_0 = 0.46 \pm 0.130$ at (1σ) confidence level [49] which has been further analyzed to $z_0 = 0.43 \pm 0.070$ at $(1\ \sigma)$ [49]. According to SNLS [50], as well as the one recently compiled in [51], the transition red-shift $z_0 \equiv 0.6$ (1σ) is in better agreement with the flat ΛCDM model $z_0 = (2\Omega_\Lambda/\Omega_m)^{1/3} - 1 \sim 0.66)$. Another limit is $0.60 \leq z_0 \leq 1.18$ $(2\sigma$, joint analysis) [52]. Further, the transition red-shift for our derived model comes to be $z_0 \cong 0.65$ for observed Hubble datasets and $z_0 \cong 1.965$ for supernovae which is in best agreement with the SNe- Ia supernovae observations, including the farthest known supernova SNI997ff at $z \approx 1.7$ [53]. We see that the variation of q with z obtained in our model is compatible with the results. In our derived model the best-fit value of deceleration parameter q_0 for Hubble and Supernova is -0.2792 , -0.4774. Figure 4 shows plot of

Preprints (www.preprints.org) | NOT PEER-REVIEWED | Posted: 8 August 2023 doi:10.20944/preprints202308.0625.v1

deceleration parameter v Redshift for both Hubble and Supernovae datasets for values of model parameters H_0, δ and λ are from Table 1.

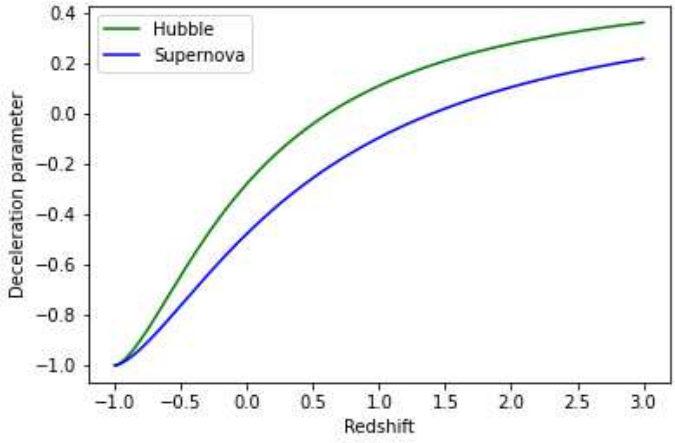

Figure 4. Behavior of (Redshift - Deceleration parameter) plane for the constant values.

Table 1. Best-fit values of model parameter H_0, δ and λ for both Datasets.

Datasets	H_0	δ	λ	ϵ
Hubble	$64.49^{+0.33}_{-0.32}$	$1.54^{+0.02}_{-0.02}$	$1.14^{+0.068}_{-0.077}$	$30.2^{+0.90}_{-0.87}$
SNe-Ia	$68.665^{+2.2}_{-2.1}$	$1.53^{+0.28}_{-0.29}$	$1.86^{+0.37}_{-0.34}$	$23.954^{+3.74}_{-2.84}$

In this study, it was argued that $\{r, s\}$ plane is useful to differentiate between various models. An analysis based on $\{r, s\}$ has also useful to differentiate between general relativity and modified theory of gravity. We note that for the Hubble datasets, the r and s parameters at the present epoch are $r_0 = 0.43987$ and $s_0 = -3.3632$ while for the SNe-Ia datasets, $r_0 = 0.48918$ and $s_0 = -10.5851$ as shown in Figure 5. Currently, observations are not sensitive enough to measure these parameters. Future data, however, could be used to infer these values, which would tremendously aid in defining the characteristics of dark energy.

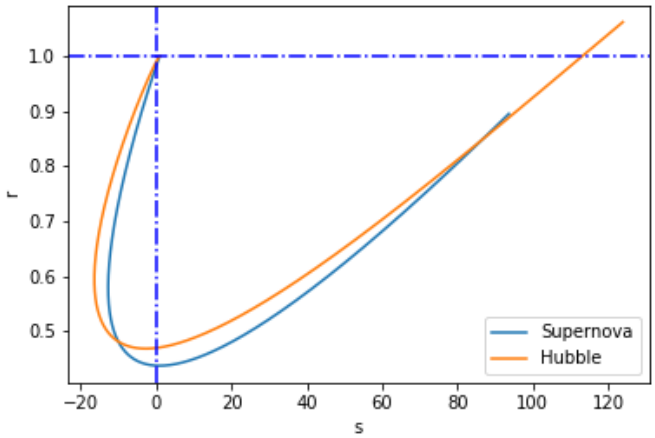

Figure 5. Behavior of $(s - r)$ plane for the constant values.

VI. Models of $f(Q, T)$ gravity

In this section, we discuss some physical aspects of different models of $f(Q, T)$ gravity

Preprints (www.preprints.org) | NOT PEER-REVIEWED | Posted: 8 August 2023 doi:10.20944/preprints202308.0625.v1

A. Model-I

Here we consider the $f(Q,T)$ gravity model as

$$f(Q,T) = a_1 Q + a_2 T, \tag{28}$$

For above model the field Equations (14)–(16), take the form

$$\rho = \frac{a_1 \dot{H}}{a_2 + 8\pi} - \frac{a_1 \left(3H^2 + \dot{H}\right)}{2\left(a_2 + 4\pi\right)}, \tag{29}$$

Figure 6 shows a plot of Pressure versus Redshift for both Hubble and SNe-Ia datasets for H_0, δ and λ are from Table 1 while model parameters a_1=-0.0125 and a_2=-0.012 respectively.

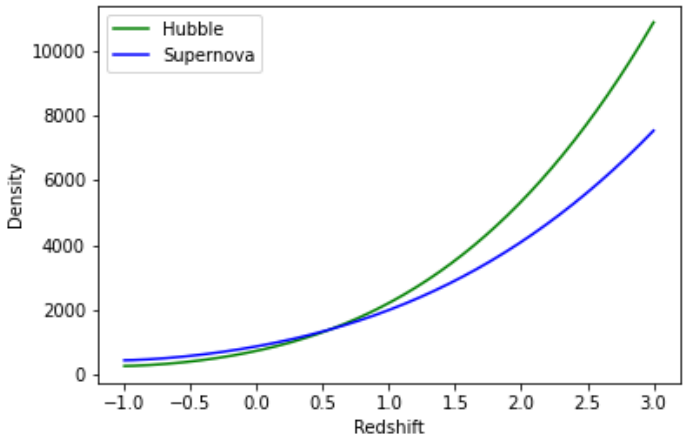

Figure 6. Behavior of (Redshift - Density) plane for the constant values ϵ,δ and λ.

$$\omega = \frac{-3a_2\left(H^2 + \dot{H}\right) - 8\pi\left(3H^2 + 2\dot{H}\right)}{a_2\left(3H^2 - \dot{H}\right) + 24\pi H^2}, \tag{30}$$

The EoS parameter is associated with energy density ρ and pressure p. The EoS parameter appears to be positive in the beginning. As a consequence, it moves from the positive region to negative region. The negative ω is proposed a constant vacuum energy density, It's worth noting that $\omega = 0$ shows Pressure-less Cold matter (PCL), $\omega = (0, \frac{1}{3})$ represents Hot matter, $\omega = \frac{1}{3}$ is radiation, $\omega = (\frac{1}{3}, 1)$ is Hard Universe, $\omega = 1$ shows stiff fluid (SF), $\omega > 1$ is Ekpyrotic matter (Ek-M), $\omega > -1$ stand for the quintessence (Q) region and $\omega < -1$ stands for the phantom region (Ph) , respectively while $\omega = -1$ represents the cosmological constant (Λ CDM) and $\omega << -1$ is precluded by SNe-Ia perceptions. Subsequently, the evolving range of ω of our derived model is supportive of (Λ CDM) model in both Hubble and supernova data.

From Figure 7, we can observe that the Universe exists the decelerated regime and enters in the accelerating phase as studied [54].

Furthermore, to verify the genuineness of model in context of cosmic acceleration, we resolve different forms of energy conditions by calculating

$$\rho + p = \frac{2a_1 \dot{H}}{a_2 + 8\pi}, \tag{31}$$

$$\rho - p = -\frac{a_1\left(3H^2 + \dot{H}\right)}{a_2 + 4\pi}, \tag{32}$$

and

$$3p + \rho = a_1\left(\frac{3H^2 + \dot{H}}{a_2 + 4\pi} + \frac{4\dot{H}}{a_2 + 8\pi}\right), \tag{33}$$

Preprints (www.preprints.org) | NOT PEER-REVIEWED | Posted: 8 August 2023 doi:10.20944/preprints202308.0625.v1

for NEC, DEC and SEC respectively. Figures 8 and 9 are plots of Energy Conditions with respect to constant obtained from best-fit for Hubble and SNe-Ia datasets as shown in Table 1 and model parameters a_1=-0.0125 and a_2=-0.012. According to the both data of the accelerating Universe, the SEC must be violated on cosmological scale [55,56]. Also, negative EoS (ω) indicate that $\rho + 3p < 0$. Therefore, there is a violation of the SEC at present. We also can see in Figure 8 and 9 that the NEC, and DEC are obeying for both Hubble and SNe-Ia datasets. Since we have shown the behavior of energy density in Figure 6. We have examined the NEC behavior (i.e., partial condition of WEC). Therefore, validation of NEC and energy density together results in the validation of WEC.

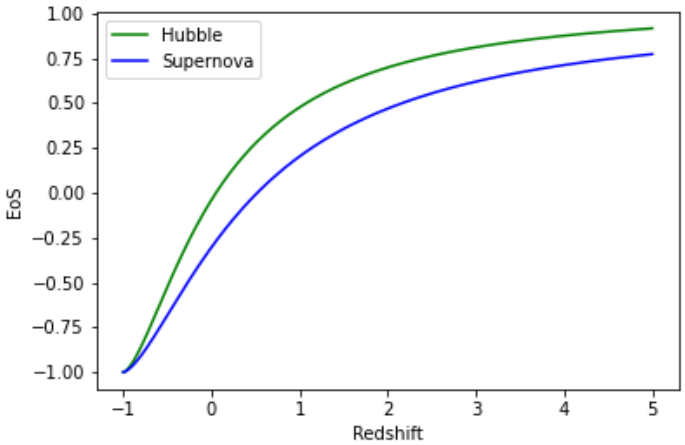

Figure 7. Behavior of (Redshidt - EoS) plane for the constant values ϵ,δ and λ.

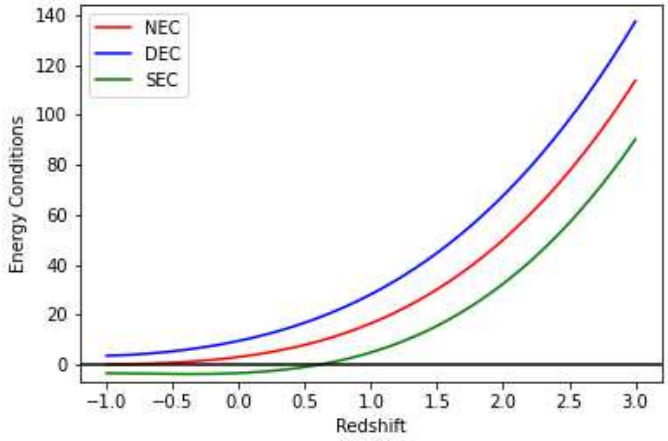

Figure 8. Behavior of (Redshift - Energy Conditions) plane for Hubble Data set.

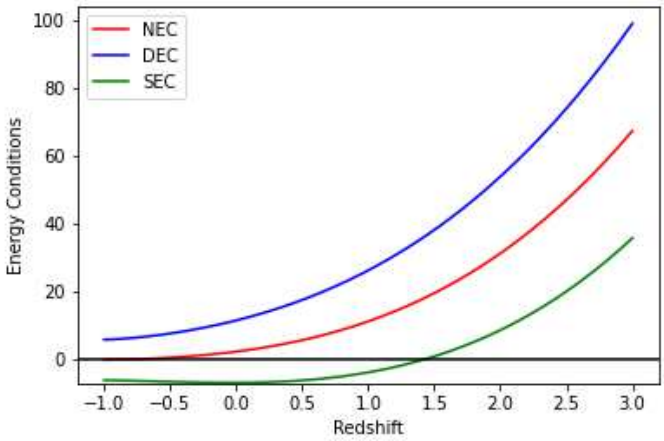

Figure 9. Behavior of (Redshift - Energy Conditions) plane for SNe-Ia Data set.

Preprints (www.preprints.org) | NOT PEER-REVIEWED | Posted: 8 August 2023 doi:10.20944/preprints202308.0625.v1

Table 2. 54 points of $H(z)$ data: 28 (DA) + 26 (BAO+other).

z	H(z)	σ_H	Ref.	z	H(z)	σ_H	Ref.
0.07	69	19.6	[57]	0.9	69	12	[58]
0.120	68.6	26.2	[57]	0.170	83	8	[59]
0.179	75	4	[60]	0.2	72.9	29.6	[57]
0.27	77	14	[59]	0.28	88.8	36.6	[57]
0.350	76.3	5.6	[61]	0.38	83	13.5	[62]
0.4	95	17	[59]	0.42	87.1	11.2	[62]
0.44	92.8	12.9	[62]	0.47	89	34	[57]
0.48	97	62	[63]	0.6	87.9	6.1	[64]
0.68	92	8	[60]	0.73	97.3	7	[64]
0.78	105	12	[60]	0.87	125	17	[60]
0.90	117	23	[59]	1.037	154	20	[60]
1.3	168	17	[59]	1.363	160	33.6	[59]
1.430	177	18	[59]	1.530	140	14	[59]
1.750	202	40	[59]	1.965	186.5	50.4	[65]
0.24	79.69	2.99	[66]	0.30	81.7	6.22	[67]
0.31	78.18	4.74	[68]	0.34	83.8	3.66	[66]
0.35	87.7	9.1	[69]	0.36	79.94	3.38	[68]
0.38	81.5	1.9	[70]	0.40	82.04	2.03	[68]
0.43	86.45	3.97	[66]	0.44	82.6	7.8	[71]
0.44	84.81	1.83	[68]	0.48	87.79	2.03	[68]
0.51	90.4	1.9	[70]	0.52	94.35	2.64	[68]
0.56	93.34	2.3	[68]	0.57	87.6	7.8	[72]
0.57	96.8	3.4	[73]	0.59	98.48	3.18	[68]
0.6	87.9	6.1	[71]	0.61	97.3	2.1	[70]
0.64	98.82	2.98	[68]	0.73	97.3	7	[71]
2.30	224	8.6	[74]	2.33	224	8	[75]
2.34	222	8.5	[76]	2.36	226	9.3	[77]

B. Model-II

Here we consider the $f(Q,T)$ gravity model as,

$$f(Q,T) = a_3Q^2 + a_4T, \tag{34}$$

For above model the field Equations (14)–(16), take the form

$$\rho = -\frac{3\left(72\pi a_3H^4 + 9a_3a_4H^4 - 2a_3a_4H^2\dot{H} - 4a_3a_4\dot{H}H^2\right)}{\left(a_4+4\pi\right)\left(a_4+8\pi\right)}, \tag{35}$$

Figure 10 shows plot of Density versus redshift for both Hubble and SNe-Ia datasets for H_0, δ and λ are from Table 1, while model parameters a_1=-0.0125 and a_2=-0.012 respectively.

$$\omega = \frac{-3a_4\left(3H^2+4\dot{H}+2\dot{H}\right) - 8\pi\left(9H^2+8\dot{H}+4\dot{H}\right)}{a_4\left(9H^2-4\dot{H}-2\dot{H}\right)+72\pi H^2}, \tag{36}$$

As shown in Figure 11, the universe is in an accelerating mode and is about to enter a decelerating phase. Additionally, we resolve various energy conditions by calculating the model's accuracy in the context of cosmic acceleration.

$$\rho + p = \frac{24a_3H^2\left(2\dot{H}+\dot{H}\right)}{a_4+8\pi}, \tag{37}$$

$$\rho - p = -\frac{6a_3H^2\left(9H^2+4\dot{H}+2\dot{H}\right)}{a_4+4\pi}, \tag{38}$$

and

$$3p + \rho = \frac{6a_3H^2\left(a_4\left(9H^2+20\dot{H}+10\dot{H}\right)+24\pi\left(3H^2+4\dot{H}+2\dot{H}\right)\right)}{\left(a_4+4\pi\right)\left(a_4+8\pi\right)}, \tag{39}$$

Preprints (www.preprints.org) | NOT PEER-REVIEWED | Posted: 8 August 2023 doi:10.20944/preprints202308.0625.v1

for NEC, DEC and SEC, respectively.

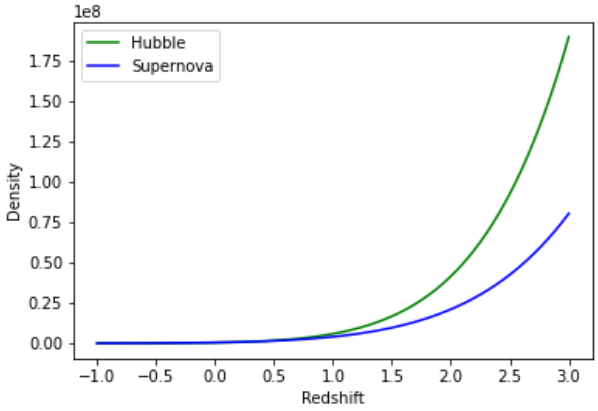

Figure 10. Behavior of (Redshift- Density) plane for the constant values ϵ,δ and λ.

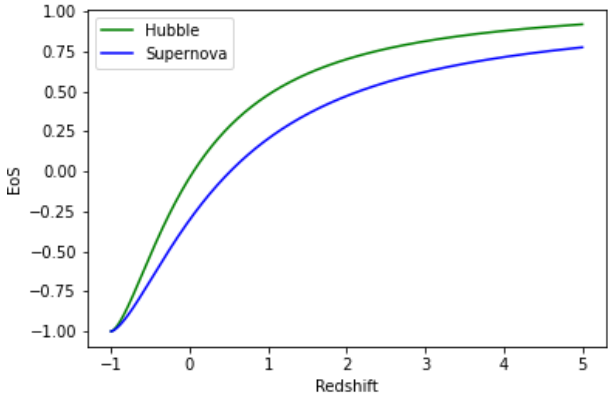

Figure 11. Behavior of (Redshift - EoS) plane for the constant values H_0,δ and λ.

For NEC, DEC and SEC respectively. Figures 12 and 13 are plots of Energy Conditions with respect to constant obtained from best-fit for Hubble and SNe-Ia datasets as shown in Table 1 and model parameters a_1=-0.0125 and a_2=-0.012. According to the both data of the accelerating Universe,as shown in 12 and Figure 13 the SEC must be violated on cosmological scale [55,56]. Also, negative EoS (ω) indicate that $\rho + 3p < 0$. Therefore, there is a violation of the SEC at present. Figures 12 and 13 indicate that the NEC, and DEC are obeying for both Hubble and SNe-Ia datasets. We have examined the NEC behavior (i.e., partial condition of WEC). Therefore, validation of NEC and energy density together results in the validation of WEC.

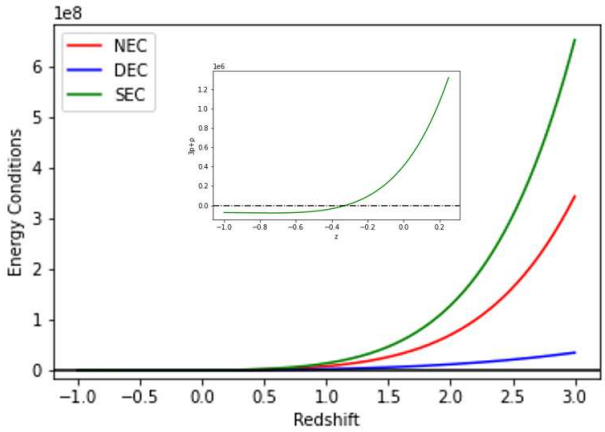

Figure 12. Behavior of (Redshift - Energy Conditions) plane for Hubble Data set for a_1=-0.0125 and a_2=-0.012.

Preprints (www.preprints.org) | NOT PEER-REVIEWED | Posted: 8 August 2023 doi:10.20944/preprints202308.0625.v1

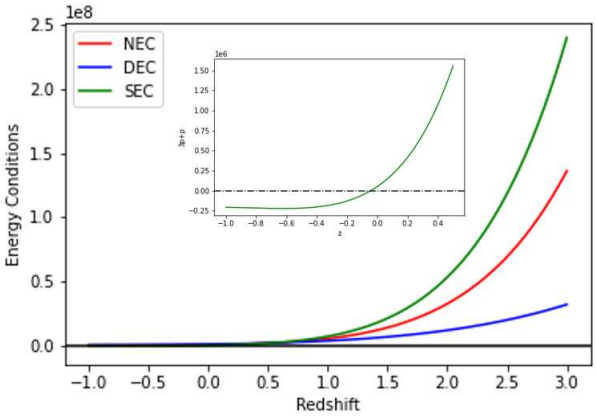

Figure 13. Behavior of (Redshift - Energy Conditions) plane for SNe-Ia Data set for a_1=-0.0125 and a_2=-0.012.

VII. CONCLUSIONS

In present work we have taken a function $f(Q,T)$ both linear and quadratic as

$$f(Q,T) = a_1Q + a_2T, f(Q,T) = a_3Q^2 + a_4T \tag{40}$$

where a_1, a_2, a_3 and a_4 are model parameters. In terms of redshift z, we have measured a number of cosmological parameters in the FLRW universe, including the Hubble parameter H and the deceleration parameter q. By applying the $R^2 - test$ formula for observational constraints on the model, we were able to determine the approximate best-fit values of the model parameters $\epsilon, \delta, \lambda,$ andH_0 utilizing datasets like the Hubble data set $H(z)$ and union 2.1 compilation of SNe-Ia datasets. The current values of the cosmological models H_0 and q_0 that we estimated are close to the values found in mainstream cosmology. Talk about EoS and the various energy conditions. Following are the characteristics of our cosmological model:

- Figures 1 and 2 provide best-fit plots based on the observed datasets. For the best fit, we employed a hybrid model combining the gradient descent and least squares approach. R^2-value for Hubble and SNe-Ia datasets are 0.9321 and 0.9930 respectively. SNe-Ia has 580 observation and giving best-fit among both datasets.
- Hubble function derived is constrained by observational datasets i.e. Hubble and SNe-Ia datasets and the present value of Hubble constant is $64.4772 km/s/Mpc$ and $68.665 km/s/Mpc$ respectively with respect to best-fit plot.
- The transition from early deceleration to the universe's present acceleration is shown by the deceleration parameter $q_0 = -0.2792$ and $q_0 = -0.4774$ with respect to Hubble and SNe-Ia datasets.
- We have considered two functional form of $f(Q,T)$ gravity in Section A , B and watched how the energy density and EoS parameter all behaved. The EoS parameter exhibits a transition from early deceleration to late time acceleration with regard to the model parameters, while the density in both models exhibits positive behavior.
- In both the functional form of $f(Q,T)$ of section A and B, NEC, WEC and DEC are satisfied whereas SEC is violated (see Figures 8, 9, 12 and 13).

Data Availability Statement: No advanced data associated with this article.

Acknowledgments: The IUCAA, Pune, India, provided the facilities and support under the Visiting Associateship Programmes, for which the authors (S. H. Shekh and A. Pradhan) are grateful.

Conflicts of Interest: The authors declared that they have neither personal relationships nor competing financial interests that could influenced the work reported in this paper.

References

1. Perlmutter, S.; Aldering, G.; Goldhaber, G.; Knop, R.A.; Nugent, P.; Castro, P.G.; Deustua, S.; Fabbro, S.; Goobar, A.; Groom, D.E.; et al. Measurements of Ω and Λ from 42 high-redshift supernovae. *Astrophys. J.* **1999**, *517*, 565–586.
2. Kamenshchik, A.Y.; Tronconi, A.; Venturi, G. Dynamical dark energy and spontaneously generated gravity. *Phys. Lett. B* **2012**, *713*, 358–364.
3. Sahni, V.; Starobinsky, A. Reconstructing dark energy. *Int. Jour. Mod. Phys. D* **2006**, *12*, 2105–2132.
4. Nojiri,S.; Odintsov, S.D.; Sasaki, M. Gauss-Bonnet dark energy. *Phys. Rev. D* **2005** *71*, 123509.
5. Buchdahl, H. A. Non-linear Lagrangians and cosmological theory, *Monthly Not. Roy. Astron. Soc.* **1970**, *150*, 1–8.
6. Dixit, A.; Bhardwaj, V.K.; Pradhan, A.; Krishnannair, S. Observational constraint in Kantoswki-Sachs f(R) gravity model with strange quark matter. *Indian J. Phys.* **2023**, http://dx.doi.org/10.1007/s12648-023-02669-0.
7. Debnath, U.; Molla, N.U.; Pradhan, A. Noncommutative wormhole in non-minimal curvature-matter coupling of $f(R)$ gravity with Gaussian and Lorentzian distributions. *Int. J. Geom. Methods Mod. Phys.* **2023**, https://doi.org/10.1142/S0219887823502146.
8. Harko, T.; Lobo, F.S.; Nojiri, S.I.; Odintsov, S.D. f (R, T) gravity. *Phys. Rev. D* **2011**, *84*, 024020.
9. Tangphati, T.; Panotopoulos, G.; Banerjee, A.; Pradhan, A. Charged compact stars with colour-flavour-locked strange quark matter in f(R,T) gravity. *Chin. J. Phys.* **2023**, *82*, 62–74.
10. Pradhan, A.; Goswami, G.K.; Beesham, A. The reconstruction of constant Jerk parameter with $f(R,T)$ gravity. *Jour. High Energy Astrophys.* **2023**, *38*, 12–21.
11. Pradhan, A.; Goswami, G.K.; Beesham, A. The reconstruction of constant Jerk parameter with $f(R,T)$ gravity in Bianchi-I spacetime. *Europ. Phys. J. Plus* **2023**, *138*, 451.
12. Pradhan, A.; Goswami, G.K.; Beesham, A. Reconstruction of an observationally constrained $f(R,T)$ gravity model. *Int. J. Geom. Methods Mod. Phys.* **2023**, 2350169. https://doi.org/10.1142/S0219887823501694.
13. Pradhan, A.; Goswami, G.K.; Beesham, A. An f(R, T) gravity based FLRW model and observational constraints. *Astronomy and Computing*, **2023**, *44*, 100737.
14. Zubair, M.; Zeeshan, M.; Hasan, S.S.; Oikonomou, V.K. Impact of collisional matter on the late-time dynamics of f(R,T) gravity, *Symmetry* **2018**, *10(10)*, 463.
15. Cai, Y.F.; Capozziello, S.; De Laurentis, M.; Saridakis, E.N. f (T) teleparallel gravity and cosmology. *Rep. Prog. Phys.* **2016**, *79*, 106901.
16. Sharif, M.; Ikram, A. Energy conditions in f (G, T) gravity, *Eur. Phys. J. C* **2016**, **76**, 640.
17. Ayuso, I.; Jimenez, J.B.; Cruz-Dombriz, A. Consistency of universally nonminimally coupled $f(R,T,R_{\mu\nu}T_{\mu\nu})$ theories. *Phys. Rev. D* **2013**, *91*, 104003.
18. Nester, J.M.; Yo, H.J. Symmetric teleparallel general relativity. 1999, *Chin. J. Phys.* **1999** *37*, 113, arXiv preprint gr-qc/9809049.
19. Pradhan, A.; D.C. Maurya; Dixit, A. Dark energy nature of viscous Universe in $f(Q)$-gravity with observational constraints. *Int. J. Geom. Method Mod. Phys.* **2021**, *18* , 2150124.
20. Banerjee, A.; Pradhan, A.; Tangphati, T.; Rahaman, F. Wormhole geometry in $f(Q)$ gravity and the energy conditions. *Europ. Phys. J. C* **2021**, *81*, 10131.
21. Dixit, A.; Maurya, D.C.; Pradhan, A. Phantom dark energy nature of bulk-viscosity universe in modified f(Q)-gravity. *Int. J. Geom. Methods Mod. Phys.* **2022**, *19*, 2250198.
22. Pradhan, A.; Dixit, A.; Maurya, D.C. Quintessence behaviour of an anisotropic bulk viscous cosmological model in modified f(Q)-gravity. *Symmetry* **2022**, *14 (12)*, 2630.
23. Gupta, S.; Dixit, A.; Pradhan, A. Tsallis holographic dark energy scenario in viscous F(Q) gravity and Tachyon field. *Int. J. Geom. Methods Mod. Phys.* **2023**, *20*, 2350021.
24. Shekh, S.H.; Bouali, A.; Mustafa, G.; Pradhan, A. Observational constraints in accelerated emergent f(Q) gravity model. *Class. Quantum Grav.* **2023**, *40*, 0555011.
25. Maurya, D.C.; Dixit, A.; Pradhan, A. Transit string dark energy models in f(Q) gravity. *Int. J. Geom. Methods Mod. Phys.* **2023**, *20*, 2350134.
26. Xu, Y.; Li, G.; Harko, T.; Liang, S. f(Q, T) gravity. *Eur. Phys. J. C* **2019**, *79*, 708.

27. Pradhan, A.; Dixit, A. The model of the transit cosmology along with observational constrictions in $f(Q,T)$ gravity. *Int. J. Geom. Method Mod. Phys.* **2021**, *18* , 2150159.
28. Shekh, S.H.; Bouali, A.; Pradhan, A.; Beesham, A. New emergent observational constraints in $f(Q,T)$ gravity model. *Jour. High Energy Astrophys.* **2023**, *39*, 53–59.
29. Xu, Y.; Harko, T.; Shahidi, S.; Liang, S. Weyl type f(Q, T) gravity, and its cosmological implications. *Eur. Phys. J. C* **2020**, *80*, 449.
30. Narawade, S.A.; Koussour, M.; Mishra, B. Constrained f(Q,T) gravity accelerating cosmological model and its dynamical system analysis. *Nucl. Phys. B* **2023**, *992*, 116233.
31. Riess, A.G.; Macri, L.; Casertano, S.; Lampeitl, H.; Ferguson, H.C.; Filippenko, A.V.; Jha, S.W.; Li, W.; Chornock, R. A 3% solution: determination of the Hubble constant with the Hubble Space Telescope and Wide Field Camera 3. *Astrophys. J.* **2011**, *730*, 119.
32. Riess, A.G.; Filippenko, A.V.; Challis, P.; Clocchiatti, A.; Diercks, A.; Garnavich, P.M.; Gilliland, R.L.; Hogan, C.J.; Jha, S.; Kirshner, R.P.; Leibundgut, B.R.U.N.O. Observational evidence from supernovae for an accelerating universe and a cosmological constant. *Astro. J.* **1998**, *116*, 1009.
33. Hawking, S.W.; Ellis, G.F.R. The large scale structure of space-time. *Cambridge University Press* (1973).
34. Wald, R.M. General Relativity. *University of Chicago Press* (1984).
35. Capozziello, S.; Nojiri, S.; Odinstov, S.D. The role of energy conditions in $f(R)$ cosmology. *Phys. Lett. B* **2018**, *781*, 99.
36. Visser, M. Energy conditions in the epoch of galaxy formation. *Science* **1997**, *276.5309*, 88-90.
37. Sharif, M.; Ikram, A. Energy conditions in $f(G,T)$ gravity, *Eur. Phys. J. C* **2016**, *76*, 640.
38. Yousaf, Z.; Sharif, M.; Ilyas, M.; Zaeem-ul-Haq Bhatti, M. Energy conditions in higher derivative $f(R,R,T)$ gravity, textitInt. J. Geom. Methods Mod. Phys. **2018**, *15*, 1850146.
39. Santos, J., Alcaniz, J.S.; Reboucas, M.J.; Carvalho, F.C. Energy conditions in $f(R)$ gravity, *Phys. Rev. D*, **2007**, *76*, 083513.
40. Atazadeh, K.; Khaleghi, A.; Sepangi, H.R.; Tavakoli,Y. Energy conditions in $f(R)$ gravity and Brans-Dicke theories, *Int. J. Mod. Phys. D*, **2009**, *18*, 1101.
41. Garcia, N.M.; Harko, T.; Lobo, F.S.N.; Mimoso, J.P. Energy conditions in modified Gauss-Bonnet gravity, *Phys. Rev. D* **2011**, *83*, 104032.
42. Liu, D.; Reboucas, M.J. Energy conditions bounds on $f(T)$ gravity, *Phys. Rev. D*, **2012**, *86*, 083515.
43. Koussour, M.; Myrzakulov, N.; Shekh, S.H.; Bennai, M. Quintessence universe and cosmic acceleration in $f(Q,T)$ gravity, *Int. Jour. Mod. Phys. D* **2022**, *31*, 2250115.
44. Arora, S.; Sahoo, P.K. Energy conditions in $f(Q,T)$ gravity, *Phys. Scr.* **2020**, *05*, 095003.
45. Freedman, W.L.; Madore, B.F.; Gibson, B.K.; Ferrarese, L.; Kelson, D.D.; Sakai, S.; Mould, J.R.; Kennicutt Jr, R.C.; Ford, H.C.; Graham, J.A.; Huchra, J.P. Final Results from the Hubble Space Telescope Key Project to Measure the Hubble Constant 2001, *ApJ* **2001**, *553*, 47.
46. Suyu, S.H.; Marshall, P.J.; Auger, M.W.; Hilbert, S.; Blandford, R.D.; Koopmans, L.V.E.; Fassnacht, C.D.; Treu, T. Dissecting the Gravitational lens B1608+656. II. Precision Measurements of the Hubble Constant, Spatial Curvature, and the Dark Energy Equation of State, *ApJ*, **2010**, *711*, 201.
47. Ade, P.A.; Barreiro Vilas, R.B.; Curto Martin, A.; Diego Rodriguez, J.M.; Gonzalez-Nuevo Gonzalez, J.; Herranz Munoz, D.; Lopez-Caniego Alcarria, M.; Martinez Gonzalez, E.; Toffolatti, L.; Vielva Martinez, P. Planck 2013 results. XVI. Cosmological parameters *A & A*, **2014**, *571*, A16.
48. Suzuki, N.; Rubin, D.; Lidman, C.; Aldering, G.; Amanullah, R.; Barbary, K.; Barrientos, L.F.; Botyanszki, J.; Brodwin, M.; Connolly, N.; Dawson, K.S. The Hubble Space Telescope Cluster Supernova Survey. V. Improving the Dark-energy Constraints above $z \geq 1$ and Building an Early-type-hosted Supernova Sample 2012, *Astrophys. J.* **2012**, *85*, 746.
49. Riess, A.G.; Nugent, P.E.; Gilliland, R.L.; Schmidt, B.P.; Tonry, J.; Dickinson, M.; Thompson, R.I.; Budavari, T.; Casertano, S.; Evans, A.S.; Filippenko, A.V. The farthest known supernova: Support for an accelerating universe and a glimpse of the epoch of deceleration, *Astrophys. J.* **2001**, *560*, 49.
50. Amara, A.; Refregier, A. Optimal surveys for weak?lensing tomography. *Month. Not. Royal Astron. Soc.* **2007**, *381(3)*, 1018–1026.
51. Davis, T.M.; Mörtsell, E.; Sollerman, J.; Becker, A.C.; Blondin, S.; Challis, P.; Clocchiatti, A.; Filippenko, A.V.; Foley, R.J.; Garnavich, P.M.; Jha, S. Scrutinizing exotic cosmological models using ESSENCE supernova data combined with other cosmological probes. *Astrophys. J.* **2007**, *666*, 716.

52. Lima, J.A.S.; Jesus, J.F.; Santos, R.C.; Gill, M.S.S. Is the transition redshift a new cosmological number ? **2012** arXiv:1205.4688v3 [astro-ph.CO].
53. Amendola, L. Acceleration at $z > 1$? *Mon. Not. R. Astron. Soc.*, **2003**, *342*, 221.
54. Capozziello, S.; Ruchika, A.; Sen, A. Model-independent constraints on dark energy evolution from low-redshift observations. *Mon. Not. Roy. Astron. Soc.*, **2019**, *484*, 4484.
55. Barcelo, C.; Visser, M. , Twilight for the energy conditions? *Int. J. Mod. Phys. D*, **2002**, *11*, 1553.
56. Moraes, P.H.R.S.; Sahoo, P.K. The simplest non-minimal matter?geometry coupling in the f(R, T) cosmology. *Eur. Phys. J. C* **2017**, *77*, 480.
57. Stephen, A.; Linder, E. V. The simplest non-minimal matter-geometry coupling in the $f(R, T)$ cosmology. *Phys. Rev. D* **2013**, *87*, 023532.
58. Simon, T.; Verde, L.; Jimenez, R. Constraints on the redshift dependence of the dark energy potential. *Phys. Rev. D* **2005**, *71*, 123001.
59. Adak, D.; Bandyopadhyay, A.; Majumdar, D. Reconstructing the equation of state and density parameter for dark energy from combined analysis of recent SNe Ia, OHD and BAO data, **2011**, *arXiv:1102,4726[astro-ph.C)]*.
60. Amendolaand, L.; Tsujikawa, S. Dark Energy: Theory and Observations, *Cambridge University Press*, **2010**.
61. Aurich, R.; Steiner, F. Dark energy in a hyperbolic universe, *Mon. Not. Roy. Astron. Soc.* **2002**, *334*, 735.
62. Moresco, M.; Cimatti, A.; Jimenez, R.; Pozzetti, L.; Zamorani, G.; Bolzonella, M.; Dunlop, J.; Lamareille, F.; Mignoli, M.; Pearce, H.; Rosati, P. Improved constraints on the expansion rate of the Universe up to $z = 1.1$ from the spectroscopic evolution of cosmic chronometers , *J. Cosmol. Astropart. Phys.* **2012**, *08*, 006.
63. Allen, S.W.; Rapetti, D.A.; Schmidt, R.W.; Ebeling, H.; Morris, R.G.; Fabian, A.C. Improved constraints on dark energy from Chandra X-ray observations of the largest relaxed galaxy clusters. *Mon. Not. Roy. Astron. Soc.*, **2008**, *383*, 879.
64. Arabsalmani, M.; Sahni, V.; Saini, T.D. Reconstructing the properties of dark energy using standard sirens. *Phys. Rev. D*, **2013**, *87*, 083001.
65. Moresco, M. Raising the bar: new constraints on the Hubble parameter with cosmic chronometers at $z \sim 2$, *Mon. Not. Roy. Astron. Soc.* **2015**, *450*, L16-L20.
66. Gaztañaga, E.; Cabre, A.; Hui, L, Clustering of luminous red galaxies- IV. Baryon acoustic peak in the line-of-sight direction and a direct measurement of $H(z)$. *Mon. Not. Roy. Astron. Soc.*, **2009**, *399*, 1663.
67. Oka, A.; Saito, S.; Nishimichi, T.; Taruya, A.; Yamamoto, K. Simultaneous constraints on the growth of structure and cosmic expansion from the multipole power spectra of the SDSS DR7 LRG sample, *Mon. Not. Roy. Astron. Soc.*, **2014**, *439*, 2515.
68. Wang, Y.; Zhao, G.B.; Chuang, C.H.; Ross, A.J.; Percival, W.J.; Gil-Marin, H.; Cuesta, A.J.; Kitaura, F.S.; Rodriguez-Torres, S.; Brownstein, J.R.; Eisenstein, D.J. The clustering of galaxies in the completed SDSS-III Baryon Oscillation Spectroscopic Survey: tomographic BAO analysis of DR12 combined sample in configuration space. *Mon. Not. Roy. Astron. Soc.* **2017**,*469*, 3762.
69. Chuang, C.H.; Wang, Y. The clustering of galaxies in the SDSS-III Baryon Oscillation Spectroscopic Survey: single-probe measurements from CMASS anisotropic galaxy clustering. *Mon. Not. Roy. Astron. Soc.*, **2013**, *435*, 255.
70. Alam, S.; Ata, M.; Bailey, S.; Beutler, F.; Bizyaev, D.; Blazek, J.A.; Bolton, A.S.; Brownstein, J.R.; Burden, A.; Chuang, C.H.; Comparat, J. The clustering of galaxies in the completed SDSS-III Baryon Oscillation Spectroscopic Survey: cosmological analysis of the DR12 galaxy sample. *Mon. Not. Roy. Astron. Soc.*, **2017** *470*, 2617.
71. Blake, C.; Brough, S.; Colless, M.; Contreras, C.; Couch, W.; Croom, S.; Croton, D.; Davis, T.M.; Drinkwater, M.J.; Forster, K.; Gilbank, D. The WiggleZ Dark Energy Survey: joint measurements of the expansion and growth history at $z < 1$. *Mon. Not. Roy. Astron. Soc.* **2012**, *425*, 405.
72. Chuang, C.H.; Prada, F.; Cuesta, A.J.; Eisenstein, D.J.; Kazin, E.; Padmanabhan, N.; Sanchez, A.G.; Xu, X.; Beutler, F.; Manera, M.; Schlegel, D.J. The clustering of galaxies in the SDSS-III Baryon Oscillation Spectroscopic Survey: single-probe measurements from CMASS anisotropic galaxy clustering. *Mon. Not. Roy. Astron. Soc.* **2013**, *433*, 3559.
73. Anderson, L.; Aubourg, E.; Bailey, S.; Beutler, F.; Bhardwaj, V.; Blanton, M.; Bolton, A.S.; Brinkmann, J.; Brownstein, J.R.; Burden, A.; Chuang, C.H. The clustering of galaxies in the SDSS-III Baryon Oscillation Spectroscopic Survey: baryon acoustic oscillations in the Data Releases 10 and 11 Galaxy samples. *Mon. Not. Roy. Astron. Soc.* **2014**, *441*, 24.

74. Busca, N. G., Baryon acoustic oscillations in the Lyα forest of BOSS quasars, *Astron. Astrop.* **2013**, *552*, A96.
75. Bautista, J.E.; Guy, J.; Rich, J.; Blomqvist, M.; Des Bourboux, H.D.M.; Pieri, M.M.; Font-Ribera, A.; Bailey, S.; Delubac, T.; Kirkby, D.; Le Goff, J.M. Measurement of baryon acoustic oscillation correlations at z=2.3 with SDSS DR12 Lyα-Forests, *Astron. Astrophys.* **2017**, *603*, A12.
76. Delubac, T.; Bautista, J.E.; Rich, J.; Kirkby, D.; Bailey, S.; Font-Ribera, A.; Slosar, A.; Lee, K.G.; Pieri, M.M.; Hamilton, J.C.; Aubourg, E. Baryon acoustic oscillations in the Lyα forest of BOSS DR11 quasars, *Astron. Astrophys.* **2015**, *574*, A59.
77. Font-Ribera, A.; Kirkby, D.; Busca, N.; Miralda-Escude, J.; Ross, N.P.; Slosar, A.; Rich, J.; Aubourg, E.; Bailey, S.; Bhardwaj, V.; Bautista, J. Quasar-Lymanα forest cross-correlation from BOSS DR11: Baryon Acoustic Oscillations. *J. Cosmol. Astropart. Phys.* **2014**, *05*, 027.